





Isothermal anionic polymerization of ϵ -caprolactam to polyamide-6: Kinetic modeling and application for production process

Samet Kurt¹  | Thomas Bratzdrum¹ | Alexander Chaloupka²  |
Siegfried Horn¹  | Judith Moosburger-Will¹ 

¹Institute of Materials Resource Management, University of Augsburg, Augsburg, Germany

²NETZSCH Process Intelligence GmbH, Selb, Germany

Correspondence

Samet Kurt, Institute of Materials Resource Management, University of Augsburg, Augsburg 86135, Germany.
Email: samet.kurt@uni-a.de

Funding information

Bayerische Staatsministerium für Wirtschaft, Landesentwicklung und Energie, Grant/Award Number: NW-1803-0013

Abstract

The in-situ anionic polymerization of ϵ -caprolactam (ϵ -CL) to polyamide-6 enables the production of large, near net shape fiber reinforced composites by thermoplastic resin transfer molding. For the propagation of the flow front as well as for the progress of the solidification, the simultaneous processes of polymerization and crystallization and the corresponding reaction kinetics play a central role. To investigate these processes, preparation of reactive mixtures consisting of ϵ -CL, activator, and initiator was carried out under inert atmosphere. A solvent-based activator and initiator were used, which hardly have been studied in the literature so far. In analogy to the resin transfer molding process, quasi-isothermal differential scanning calorimetry measurements were performed at various temperatures and the released enthalpy and the degree of crystallization were determined. From these isothermal measurements, a two-stage semi-empirical kinetic model was established for a solvent-based system for the first time, which reproduces the experimental data with high precision. To apply the obtained kinetic model to a thermoplastic resin transfer molding process it was finally correlated to dielectric sensor data, allowing real-time prediction of the total conversion.

KEYWORDS

dielectric properties, differential scanning calorimetry (DSC), kinetics, polyamides, ring-opening polymerization

1 | INTRODUCTION

Polymer injection processes enable to increase the degree of automation in the production of fiber reinforced composites and thus to improve the efficiency of the value chain. In this processes, dry semi-finished fiber products

are infiltrated in a mold with a reactive, commonly thermoset polymer system and cured at specific temperatures. The use of thermoplastic matrix systems offers some advantages over thermosets for composite materials, such as a higher toughness, the possibility of forming, welding, and recycling. However, thermoplastic melts cannot be

This is an open access article under the terms of the [Creative Commons Attribution-NonCommercial-NoDerivs](https://creativecommons.org/licenses/by-nc-nd/4.0/) License, which permits use and distribution in any medium, provided the original work is properly cited, the use is non-commercial and no modifications or adaptations are made.

© 2023 The Authors. *Journal of Applied Polymer Science* published by Wiley Periodicals LLC.

used to fully impregnate dry fiber semi-finished products due to their high melt viscosity, which is often several orders of magnitude higher than the viscosity of uncured thermosetting resins. To overcome these challenges, instead of the high-viscosity thermoplastic melt, a low-viscosity monomer melt is mixed with suitable additives and injected into the mold, where in-situ polymerization takes place.¹⁻³ Due to the initially low-viscosity, complete impregnation of the fibers can be realized without high processing pressures even for large components.

Driven by cost and introduction of composite-based components with reduced mechanical requirements in the automotive and aerospace industries, a number of engineering polymers are coming into focus. A prominent example is semi-crystalline polyamide-6 (PA6), which can be produced by anionic ring-opening polymerization of the monomer ϵ -caprolactam (ϵ -CL). In this process, an initiator and an activator are used to start and accelerate polymerization, respectively, with the anionic polymerization taking place at temperatures of about 160°C within a few minutes, that is, the reaction takes place at temperatures below the melting temperature of PA6 of 220°C. The monomer system is characterized by an extremely low melt viscosity of about 5 mPa·s at 100°C,^{4,5} which renders it ideally suitable for injection processes such as thermoplastic resin transfer molding (T-RTM).^{1-3,6}

To carry out such a T-RTM process efficiently, an understanding of the reactive behavior of the starting material is essential. For in-situ polymerization of ϵ -CL, the reaction kinetics and the development of viscosity during anionic polymerization play a central role. The kinetics of the anionic polymerization of ϵ -CL to PA6 is complicated due to the simultaneous processes of polymerization and crystallization. Furthermore, the chemical composition of the reactive mixture consisting of ϵ -CL, initiator, and activator, as well as the process temperature strongly influence the reaction kinetics and the polymer characteristics.⁷⁻¹⁸ In addition, a deactivating influence of moisture on anionic polymerization is known to occur.¹⁹⁻²² Also, a high process temperature accelerates the polymerization and at the same time slows down the crystallization while a low process temperature leads to a fast crystallization, which in turn causes a slow polymerization.^{7,23}

Differential scanning calorimetry (DSC)^{9,12,24} or adiabatic reactors^{10,13,25} are commonly used to study the kinetics of the anionic polymerization of ϵ -CL to PA6. Here, we prefer the DSC approach because it enables a separation of the processes of polymerization and crystallization. Furthermore, it is possible to determine reaction and melt enthalpies precisely and therefore conclusions about the polymer properties, such as the degree of crystallization, can be drawn.

The kinetic models used so far in the literature to describe the anionic polymerization of ϵ -CL to PA6 have been summarized by Ageyeva et al.²⁶ Anionic polymerization can be described in two ways, that is, by mechanistic and semi-empirical models. The mechanistic approach²⁷⁻³¹ takes into account all chemical side reactions and is of low practicability due to the complex chemistry of anionic polymerization. The semi-empirical approach³²⁻³⁸ describes the polymerization process phenomenologically and summarizes all reactions. It is commonly used for the kinetic description of anionic polymerization. For kinetic modeling, it is assumed that the temporal change of a measurand corresponds to the reaction rate of a chemical process. In the modeling of a DSC measurements, for example, it is assumed that the amount of heat released in an exothermic polymerization reaction is directly proportional to the conversion.³⁹ Most models have the form of Equation (1), where the reaction rate is defined as the change in conversion α over time.

$$\frac{d\alpha(T,t)}{dt} = k(T)f(\alpha(t)), \quad (1)$$

Here, $k(T)$ describes the temperature dependent reaction rate and is defined by the Arrhenius temperature dependence and $f(\alpha)$ describes the reaction model. There are different phenomenological models, which describe the polymerization process of the anionic polymerization of ϵ -CL, such as the Malkin,^{33,35,36,40,41} Camargo,⁴² Lin,³⁰ and the Kamal-Sourour model^{37,38} proposed by Teuwen et al.²⁵

The crystallization mechanism for anionic polymerization is related to that of crystallization from a melt. Based on the classical models for melt crystallization,⁴³⁻⁴⁶ some further advanced crystallization models have been proposed, such as the Avrami-Kolmogorov equation by Bolgov et al.³² the Malkin model,^{33,47-49} and the Lee-Kim model.⁵⁰ Further, the differential Nakamura model⁵¹⁻⁵³ was used by Vicard et al.^{12,54} which is a generalized form of the Avrami-Kolmogorov equation. This equation is also referred to as the Johnson-Mehl-Avrami-Kolmogorov (JMAK) equation.

To perform a simple description of anionic polymerization, it can be assumed that polymerization and crystallization occur in parallel and independently of each other.²⁴ The total heat flow released during synthesis is then the sum of the heat flow of the polymerization and crystallization processes. However, this simplification does not accurately describe the physicochemical processes, since polymerization and crystallization are correlated.³³ To represent this correlation, it has been proposed that the crystallinity $\beta(t)$ is coupled to the conversion $\alpha(t)$.^{32,33} This relationship is shown in Equation (2), where $\phi(t)$ (W/g) is the total heat flow

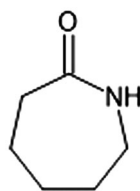


FIGURE 1 ϵ -caprolactam.

while Q_P and Q_C (J/g) are the total polymerization and crystallization enthalpy, respectively.

$$\phi(t) = Q_P \frac{d\alpha(t)}{dt} + Q_C \frac{d\beta(t)}{dt} \alpha(t). \quad (2)$$

The aim of this work is to develop for the first time a kinetic model for the anionic polymerization of ϵ -CL applying a solvent-based initiator and activator. The reactive mixture was prepared under inert gas atmosphere and the reaction as well as the crystallization enthalpies of the synthesized PA6 were accurately determined using DSC. Following the isothermal T-RTM process, special isothermal DSC temperature programs were defined. Following Equation (2), a semi-empirical approach with a two-step model A–B–C was chosen for kinetic modeling, in which the first step A–B represents the polymerization and the second step B–C the crystallization, which means that only previously polymerized parts can crystallize. In accordance with Teuwen et al.²⁵ the Kamal-Sourour and the Avrami model were applied for polymerization and crystallization, respectively.

Dielectric measurements give information about the polarizability and the ion viscosity of a polymer. The developed kinetic model was combined with signals of dielectric sensors, which monitor the anionic polymerization during T-RTM in a production environment. The resulting real-time prediction of the degree of total conversion can demonstrate the applicability of the model on large scale.

2 | EXPERIMENTAL

2.1 | Materials

Samples were prepared in a glovebox under nitrogen inert gas to prevent a contamination with water of the starting materials of the anionic polymerization of ϵ -CL. Solvent-based additives from the manufacturer Katchem spol. s r. o., that is, the initiator sodium dicaprolactamato-bis-(2-methoxyethoxy)-aluminum (dilactamate) dissolved in toluene and the activator hexamethylene diisocyanate (U7), were used. The monomer was supplied by

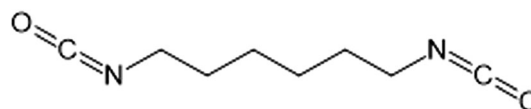


FIGURE 2 Hexamethylene-1,6-diisocyanate (U7).

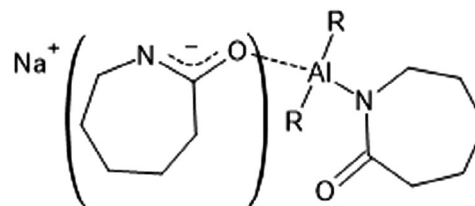


FIGURE 3 Sodium dicaprolactamato bis-(2-methoxyethoxy) aluminate²⁶ (dilactamate[®]).

Brüggemann Chemical in form of ϵ -CL flakes (AP-Nylon[®]). The structures of the respective molecules are given in Figures 1–3. The exact concentrations according to the data sheet for dilactamate are about 82 wt% of sodium dicaprolactamato bis-(2-methoxyethoxy) aluminate, about 14 wt% of toluene, and about 4 wt% of ϵ -CL. The concentrations of U7 are about 75 wt% of hexamethylene-1,6-diisocyanate homopolymer, about 12 wt% of xylenes, about 13 wt% of 2-methoxy-1-methylethyl acetate, about 0.5 wt% of hexamethylene-1,6-diisocyanate, and about 3 wt% of ethylbenzene.

To prepare a reactive mixture, about 40 g of ϵ -CL were weighed in a beaker. To ensure good thermal equilibrium between the beaker, which was sealed with a silicon stopper, and a magnetic stirrer hot plate, the beaker was placed in a hollow copper cylinder. The hot plate was adjusted to 80°C, which is just above the melting temperature and below the polymerization temperature of ϵ -CL. After 60 min, the ϵ -CL had completely melted and defined amounts of initiator and activator were added using disposable syringes. A reactive mixture of 92.5 wt% ϵ -CL, 5 wt% initiator dilactamate, and 2.5 wt% activator U7 was prepared, which was labeled KC-50-25. After the liquid reactive mixture became homogeneous, that is, no additive residue was observed, it was poured into an aluminum sheet featuring 48 molds and quenched to room temperature. The resulting solid mixture remains reactive to almost 100%. To investigate the reactivity, DSC measurements were carried out at a fresh mixture and a mixture held at 80°C for 5 h. No significant change in reactivity was observed. This procedure resulted in cylinder shaped samples of 3.5 mm in diameter and 2.0 mm in height and with a mass of about 10 mg, which were used for DSC measurements. The reactive cylindrical samples were placed in crucibles of known

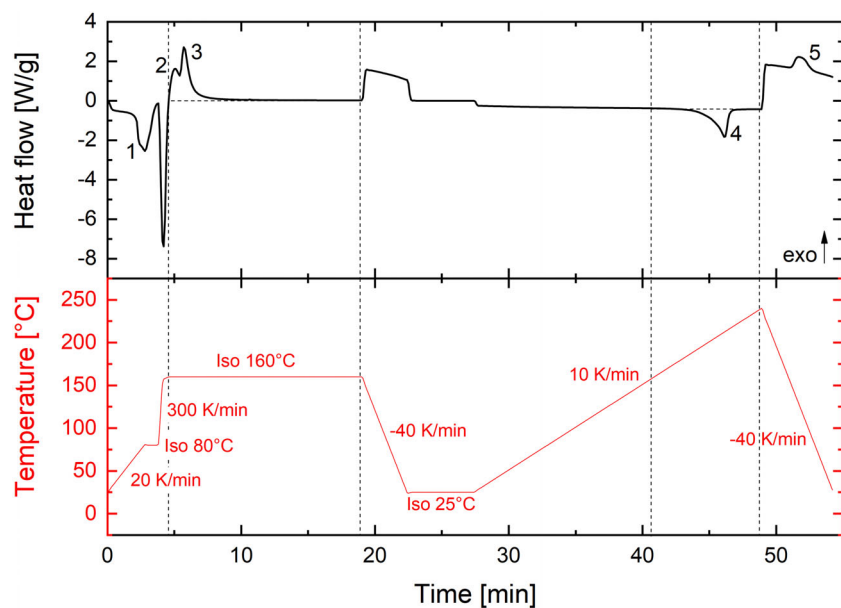


FIGURE 4 Exemplary differential scanning calorimetry (DSC) signal and corresponding temperature program for a quasi-isothermal DSC measurement with a reaction temperature of 160°C: (1) melting of reactive mixture, (2) anionic polymerization, (3) crystallization, (4) melting of PA6, and (5) recrystallization of PA6. [Color figure can be viewed at [wileyonlinelibrary.com](https://onlinelibrary.wiley.com/doi/10.1002/app.54320)]

weight and closed inside the glovebox. Therefore, the samples were protected against the influence of humidity or reactive gases. An empty DSC reference crucible was sealed under identical initial conditions. The pressed DSC crucibles were then removed from the glovebox and reweighed to determine the exact sample mass.

2.2 | Differential scanning calorimetry

Quasi-isothermal DSC measurements were performed using a DSC 214 Polyma (Netzsch, Germany). Figure 4 shows an exemplary DSC signal (top) and the corresponding temperature program (bottom) of such a quasi-isothermal DSC measurement with a target temperature of 160°C. The sample was first heated from 25 to 80°C at a heating rate of 20 K/min and kept isothermal for 1 min. During this process, the reactive mixture melts, which represents an endothermic process ((1) in Figure 4). Then the sample was heated from 80°C to the desired target temperature of 140, 145, 150, 155, 160, or 165°C, respectively, with a heating rate of 300 K/min. The target temperature was kept constant for 15 min, that is, an isothermal segment was added. The high heating rate of 300 K/min allows the anionic polymerization to be carried out under quasi-isothermal conditions, since the heating interval is much shorter than the polymerization time. For this short heating segment, the control parameters of the DSC were chosen to avoid an overshooting of the temperature but to quickly reach the target temperature. At the target temperature, exothermic anionic polymerization (2) and crystallization (3) begin and PA6 is

formed.^{18,25} In the following, the target temperature is labeled reaction temperature and refers to the temperature where both polymerization and crystallization occur. After the isothermal interval, the synthesized PA6 was cooled to 25°C at -40 K/min and kept under isothermal conditions for another 5 min. This was followed by a dynamic heating segment, in which the sample was reheated to 240°C at 10 K/min. This latter heating segment is used to confirm the complete anionic polymerization and to determine the crystallinity using the endothermic melting process of the PA6 (4). In the last step, the sample cooled down in a controlled manner at -40 K/min and the PA6 melt solidified and crystallized (5).

The enthalpy was calculated from the area between the DSC signal and a linear baseline between two defined temperature limits (see dotted lines in Figure 4). From the isothermal segment, the enthalpy of reaction ΔH_R was determined, which is composed of the heat of polymerization ΔH_P (2) and crystallization ΔH_C (3). Here, the high temperature limit of the baseline was placed at the end of the isothermal segment and a horizontal line was drawn from this point. The intersection of this line with the DSC signal corresponded to the low temperature boundary. For the dynamic heating segment at 10 K/min, the limits for each curve were determined individually based on the zero points of the first derivative of the DSC signal. The melting enthalpy or enthalpy of fusion of PA6 $\Delta H_{m,PA6}$ was determined by the area between the melting curve of the synthesized PA6 and the baseline (4).

We assume that the enthalpy of crystallization agrees with the melt enthalpy of PA6 measured reheating the

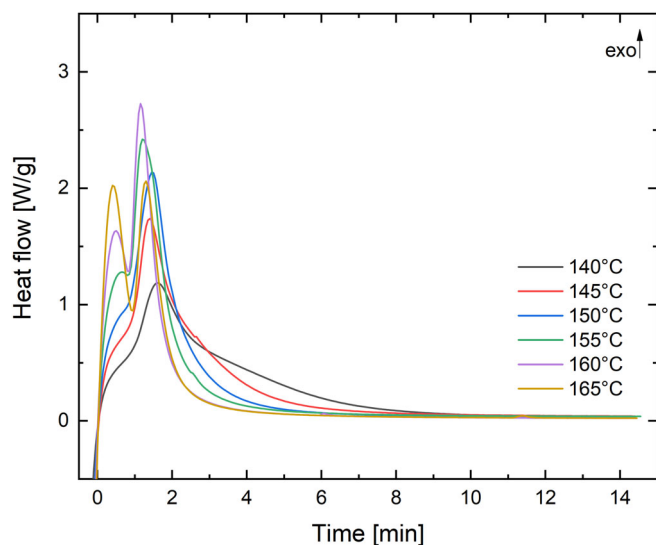


FIGURE 5 Quasi-isothermal DSC measurements with different reaction temperature for KC-50-25. [Color figure can be viewed at wileyonlinelibrary.com]

sample to 240°C.²³ Using this relationship, the polymerization enthalpy ΔH_P was calculated from the difference of the reaction enthalpy ΔH_R and the crystallization enthalpy ΔH_C , which is described by Equation 3.

$$\Delta H_P = \Delta H_R - \Delta H_C = \Delta H_R - |\Delta H_{m,PA6}|. \quad (3)$$

The crystallinity of PA6 can be determined from the enthalpy of fusion by relating this value to the theoretical enthalpy of fusion of 240 J/g, which is characteristic for a PA6 with 100% crystallinity.^{55–58}

2.3 | Dielectric measurements

Dielectric analysis (DEA) was performed using the measuring system sensXPRT Digital Mold from Netzsch Process Intelligence consisting of TMM 3c/3R sensors and the DEA 288 Ionic dielectric analyzer, which can measure in a frequency range from 1 to 1 MHz. The sensors are also suitable for temperatures up to 280°C and pressures up to 300 bars. Further information concerning the measurement process is given below.

3 | RESULTS

3.1 | Influence of reaction temperature on anionic polymerization

Figure 5 shows the DSC signals of the reactive mixture KC-50-25 taken during the isothermal segment for

different reaction temperatures. The curves exhibit two maxima due to polymerization and crystallization and then approach the baseline. A strong temperature dependence is observed. With increasing temperature, the curves approach the base line earlier, that is, polymerization and crystallization proceed faster. For reaction temperatures of 165 and 160°C, respectively, the reaction is completed after about 3 min, whereas for a temperature of 140°C about 7 min are required. Furthermore, with increasing reaction temperature, the polymerization and crystallization peaks become more pronounced and the ratio of the two peak heights changes. At low temperatures, only one pronounced (second) peak is observed. With increasing temperature, the relative height of the first peak increases.

The enthalpy as well as the degree of crystallization resulting from evaluation of the quasi-isothermal DSC measurements on KC-50-25 are shown in Figure 6. For the reaction temperature of 160°C, a total of seven measurements were performed under identical conditions to determine the statistical deviations of the DSC analysis. The measurements showed a standard deviation of 1%, which was estimated for all other reaction temperatures. The enthalpy of reaction amounts to 206 J/g for the lowest reaction temperature of 140°C, it increases slightly with increasing temperature to a maximum of 211 J/g for 150°C, and finally decreases to 190 J/g for the highest reaction temperature of 165°C. The enthalpy of fusion decreases with increasing reaction temperature. It amounts to 144 J/g for 140°C and decreases steadily to 99 J/g for 165°C. The enthalpy of polymerization resulting from the difference between these two quantities, first increases from 92 J/g for a reaction temperature of 140°C to a maximum of 102 J/g for 155°C and then decreases to 91 J/g for the highest temperature of 165°C. The degree of crystallinity is determined by the enthalpy of fusion and steadily decrease from about 48% for 140°C to 41% for 165°C.

The reaction temperature strongly influences the polymerization and crystallization processes. With increasing reaction temperatures, anionic polymerization proceeds faster while crystallinity decreases, in agreement with data from literature.^{7,23}

The crystallization process has been described, for example, by Vicard et al.²³ and Komoto et al.⁵⁹ The prerequisite for crystallization is the formation of oligomers, which act as nucleators for crystallization.

At low temperatures, anionic polymerization proceeds slowly, leaving the oligomers very mobile in the low-viscosity reactive mixture with high ϵ -CL content. This facilitates alignment of the oligomers relative to each other in the highly supercooled system. This situation results in a high crystallization rate and large and stable lamellae,

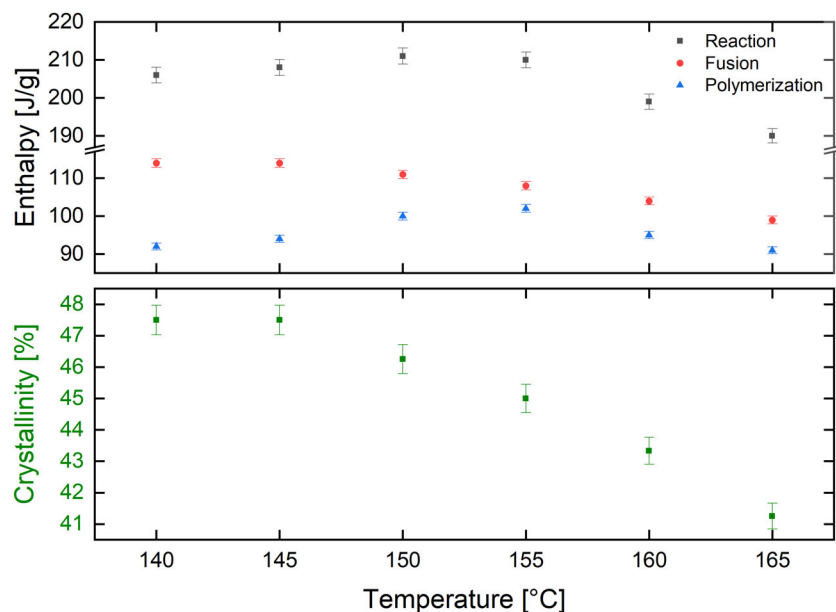


FIGURE 6 Enthalpies of reaction, fusion, and polymerization, as well as crystallinity for different reaction temperatures for KC-50-25. [Color figure can be viewed at [wileyonlinelibrary.com](https://onlinelibrary.wiley.com/doi/10.1002/app.54320)]

which increase the enthalpy of fusion.²³ Polymerization then continues at the chain ends in the crystalline phase and the growth of the lamellae continues, for example, by folding of the growing polymer chains.⁵⁹ The described process corresponds to the observed high enthalpies of fusion and concomitant high crystallinity in the range of low reaction temperatures. However, large crystallization rates can result in the trapping of reactive species, such as ϵ -CL anions, thus reducing conversion.^{17,60} This could contribute to the observed low enthalpy of polymerization for low reaction temperatures.

At high reaction temperatures the polymerization rate increases, as indicated by the time dependence of the DSC curves, and the degree of crystallization decreases. These processes explain the decrease of the reaction enthalpies for higher reaction temperatures. This might be due to the decreased mobility of the oligomers resulting from an further advanced growth process of the polymer chains and the increased viscosity of the medium.¹⁴ Increased branching can also occur in the polymer chains at this temperature, which additionally interferes with crystallization.⁷

In the literature, a maximum for the conversion is reported between 150 and 155°C,^{7,16} which is in good agreement with the observed maximum of the polymerization enthalpy at 155°C.

3.2 | Kinetic model of the isothermal anionic polymerization process

In order to set up a kinetic model of a chemical reaction, the amount of released heat $Q(t)$ as measured by DSC is

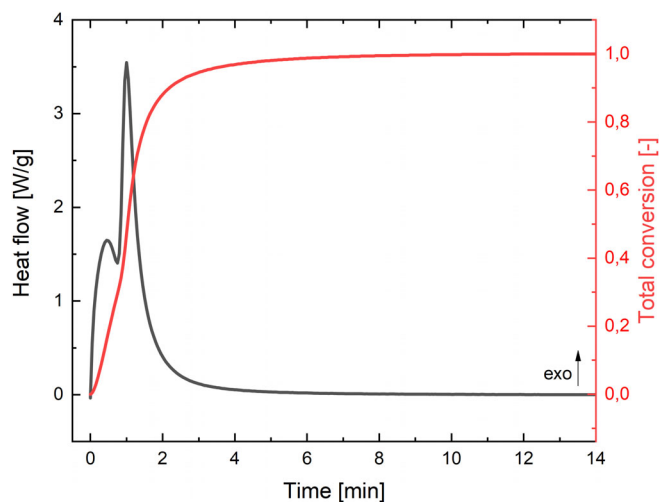


FIGURE 7 DSC signal and corresponding total conversion for KC-50-25 with a reaction temperature of 160°C. [Color figure can be viewed at [wileyonlinelibrary.com](https://onlinelibrary.wiley.com/doi/10.1002/app.54320)]

assumed to be directly proportional to the conversion $\alpha(t)$ in an exothermic polymerization reaction.³⁹ Since both polymerization and crystallization contribute to the DSC signal at a time t , the fit of the model to the DSC signal integrated over time was performed. This integrated DSC signal corresponds to the amount of heat $Q(t)$ released up to the time t . $Q(t)$ defines a total conversion of the reaction $\Omega(t)$, which consists of the sum of the conversion of the polymerization and the crystallization of the polymer (see Equation 4). Here, Q_R is the total enthalpy of reaction released, that is, the DSC signal integrated over the complete polymerization and crystallization peaks.

$$\Omega(t) = \frac{Q(t)}{Q_R} \quad (4)$$

For the kinetic modeling, the temperature program of the isothermal DSC measurements was further optimized. In order to reduce the effect of thermal inertia on the fast-heating process at 300 K/min, the sample is exposed to the temperature program consisting of the fast-heating process at 300 K/min and the isothermal segment twice in succession. After differencing the DSC signals of the two runs, the influence of the thermal inertia of the samples can be eliminated. Furthermore, nearly identical sample masses were used for the isothermal DSC measurements, which minimizes a methodical influence of the DSC on the measurement results. Figure 7 shows an example of the corrected DSC signal for KC-50-25 at 160°C isothermal reaction temperature and the corresponding total conversion.

To develop the isothermal reaction model, only the reaction regions of the isothermal DSC measurements with a target temperature of 145, 150, 155, and 160°C were considered. Due to the simultaneous polymerization and crystallization, a semi-empirical approach with a two-step model A–B–C was chosen, where the first step (A–B) represents the polymerization and the second step (B–C) represents the crystallization. Following Teuwen et al.²⁵ a polymerization model in the form of the Kamal-Sourour equation was applied for the first step (A–B) and a crystallization model in the form of the JMAK equation was used for the second step (B–C). The total heat flux $\phi(t)$ as function of time can then be written as shown in Equation (5). This total heat flux describes the measured DSC signal and the reaction rate, originating from polymerization and crystallization. Equation (5) takes into account that the crystallization process cannot proceed until initial polymer chains have been formed.

$$\phi(t) = Q_R \left[c_1 \frac{d(A \rightarrow B)}{dt} + c_2 \frac{d(B \rightarrow C)}{dt} \right], \quad (5)$$

$$\text{Polymerization: } \frac{d(A \rightarrow B)}{dt} = k_1 A^{\tilde{n}} + k_2 A^{\tilde{n}} B^{\tilde{m}},$$

$$\text{Crystallization: } \frac{d(B \rightarrow C)}{dt} = k_3 n B [-\ln(B)]^{\frac{n-1}{n}},$$

$$\text{with } k_i = p_i \exp\left(\frac{-E_i}{RT}\right).$$

The concentrations of monomer and polymer molecules are abbreviated as A and B , respectively, while C represents the fraction of the crystalline phase. The partial reaction orders are \tilde{n} and \tilde{m} , n is the Avrami

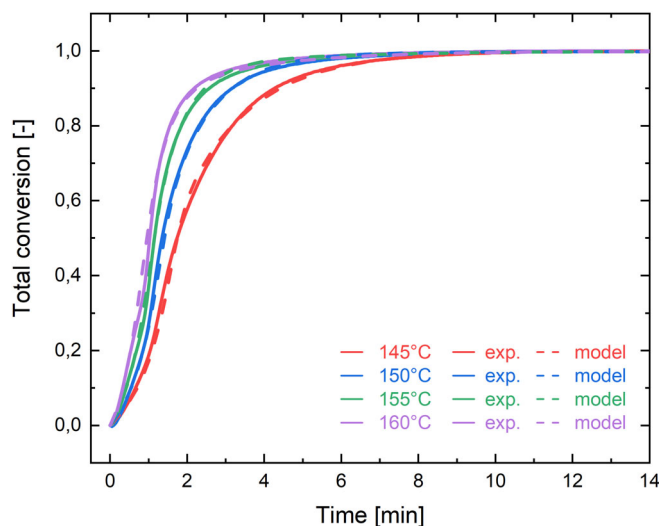


FIGURE 8 Fitting of the total experimental conversion $\Omega(t)$ of the isothermal DSC measurements for KC-50-25 with the two-step kinetic model consisting of Kamal-Sourour and JMAK ($\phi(t)/Q_R$). [Color figure can be viewed at wileyonlinelibrary.com]

TABLE 1 Calculated parameters for the two-step kinetic model consisting of Kamal-Sourour and JMAK for the isothermal DSC measurements on KC-50-25.

A-B: Kamal-Sourour		B-C: JMAK	
E_1 (kJ/mol)	77.4	E_3 (kJ/Mol)	134.1
p_1 (s ⁻¹)	$1.8 \cdot 10^7$	p_3 (s ⁻¹)	$5.3 \cdot 10^{14}$
\tilde{n} (-)	1.1	n (-)	1.0
p_2 (s ⁻¹)	$1.8 \cdot 10^7$	c_2 (-)	0.53
\tilde{m} (-)	2.2		
E_2 (kJ/mol)	72.1		
c_1 (-)	0.47		

constant, and c_1 and c_2 are weighting factors, respectively. The optimization of the two-step model was performed after entering the starting parameters using the least squares method. To facilitate the convergence of the model to the measured data, parameter bounds were defined. Values were further specified for the weighting factors c_1 and c_2 , which were derived from the average of the ratios of polymerization enthalpy and crystallization enthalpy derived for the isothermal temperatures used. The fitting results for the isothermal reaction model are shown in Figure 8. The experimental data of the total conversion $\Omega(t)$ are reproduced in very good agreement by the isothermal reaction model with a correlation coefficient of 0.97.

The corresponding fit parameters for the two-step isothermal reaction model are listed in Table 1. Considering the polymerization, in the Kamal-Sourour equation the

pre-exponential factors p_1 and p_2 are identical. The value is $1.8 \cdot 10^7 \text{ s}^{-1}$ and describes the number of collisions of the molecules during a chemical reaction.

For the non-autocatalytic part of the Kamal-Sourour equation, a first-order reaction results with \tilde{n} of 1.1. The activation energy E_1 is 77.4 kJ/mol. The autocatalytic part of the Kamal-Sourour equation has a reaction order \tilde{m} of 2.2 and the activation energy E_2 here is 72.1 kJ/mol. Overall, the total order of the reaction is 3.3. The autocatalytic part of the polymerization lies at a slightly lower activation energy compared to the first-order reaction pathway. In the literature, activation energies for anionic polymerization using sodium caprolactamate as initiator are reported in the range of 59–92 kJ/mol,^{13,25,27,29,32,36,50,61} consistent with our result. The Arrhenius terms describe the temperature dependence of the reaction rate and represent a constant at a fixed temperature. At a reaction temperature of 160°C, values for k_1 of $8.6 \cdot 10^{-3} \text{ s}^{-1}$ for the first-order reaction and for k_2 of $3.7 \cdot 10^{-2} \text{ s}^{-1}$ for the autocatalytic part result. The rate constant of the autocatalytic part of the polymerization is about four times larger than that of the first-order reaction for a temperature of 160°C. For crystallization, which is described by the JMAK equation, the activation energy is 134.1 kJ/mol and is about twice as large as the activation energies for polymerization. The Avrami constant n is 1.0 and the Arrhenius term k_3 for 160°C results in $3.5 \cdot 10^{-2} \text{ s}^{-1}$.

In the following we want to compare our results to those of Teuwen et al.²⁵ The parameters of the Kamal-Sourour equation for polymerization fitted here are of the same order of magnitude and partially in agreement with the parameters of Teuwen et al., although the additives used and the reaction conditions are significantly different. Teuwen et al. carried out the anionic polymerization in an adiabatic reactor and used 1,2 mol-% sodium caprolactamate as initiator and 1,2 mol-% hexamethylene-1,6-dicarbonyl caprolactam as activator. Even though different additives are used, the concentration of the reactive species of KC-50-25 in the present work is almost identical. For the nonautocatalytic part of the Kamal-Sourour equation, Teuwen et al. give a reaction order for \tilde{n} of 1.2 with an activation energy of 68.6 kJ/mol. The reaction order of the autocatalytic part \tilde{m} is 1.6 and the activation energy for this is 59.4 kJ/mol. Overall, the total order of the reaction is 2.8. The autocatalytic part of the polymerization lies at a lower activation energy than of the nonautocatalytic part, in agreement with our results. However, the reported activation energies of Teuwen et al. are somewhat lower. The Arrhenius term for the nonautocatalytic part of the reaction has a value for k_1 of $2.9 \cdot 10^{-3} \text{ s}^{-1}$ and for k_2 of $3.8 \cdot 10^{-2} \text{ s}^{-1}$ for the autocatalytic part for the temperature of 160°C. Thus, the rate

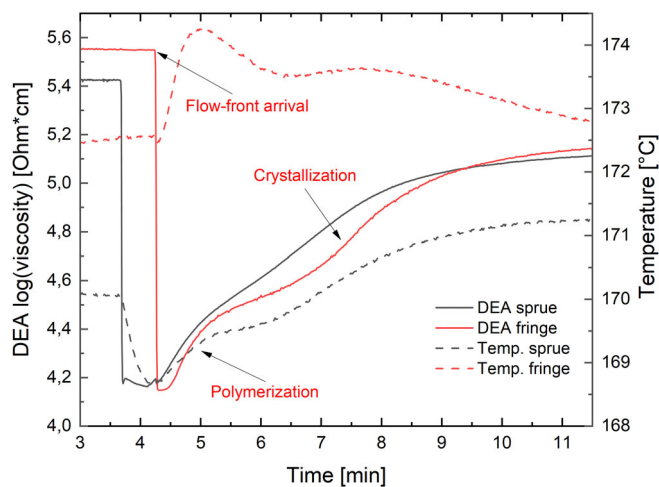


FIGURE 9 Dielectric monitoring of polymerization and crystallization during the T-RTM process at the sprue and at the fringe of the mold: ion viscosity as function of time at 100 kHz. [Color figure can be viewed at wileyonlinelibrary.com]

constant of the autocatalytic part of the polymerization is about an order of magnitude larger than that of the non-autocatalytic part. Compared with our isothermal reaction model, the rate constants of the autocatalytic part of the Kamal-Sourour equation k_2 are almost identical and those of the non-autocatalytic part k_1 are of the same order of magnitude. In particular, the agreement of k_2 confirms the theoretical assumptions of the Kamal-Sourour model that the reaction mechanism for chain growth, and thus for the rate constant for the autocatalytic part of polymerization, should be independent of the initiator and activator used.⁶²

3.3 | Application of the kinetic model in a production environment

The kinetic model, developed in a laboratory scale study, can be applied to monitor the polymerization and crystallization process in a production environment in real time. To this end, it has been combined with the signal of dielectric sensors. This allows to calculate the degree of total conversion in real-time. Such real-time monitoring allows an online control of the process parameters, for example, the conversion and the temperature. Therefore, a correlation between the process parameters and the quality of the sample is achieved. In addition, the in-situ monitoring allows a validation of our thermochemical modeling in real industrial processing environments.

A dielectric measurement monitors the microscopic properties of a polymer such as dipole–dipole interactions and the mobility of molecular chains. An alternating voltage is applied across the dielectric sensor, which induces

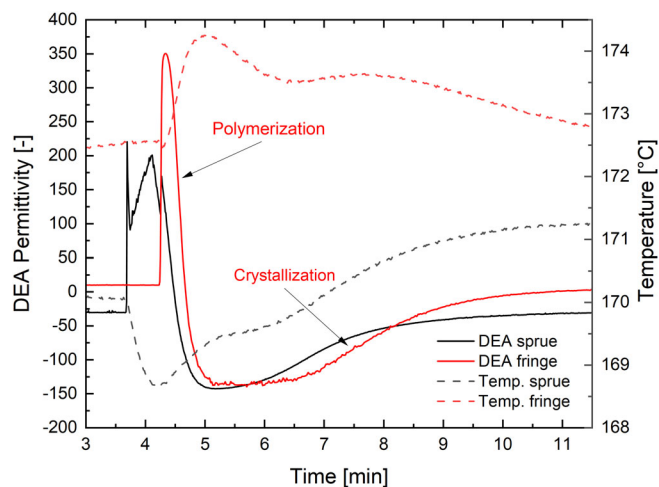


FIGURE 10 Relative permittivity at 100 kHz during the T-RTM process at the sprue and at the fringe of the mold (uncalibrated measurement). [Color figure can be viewed at [wileyonlinelibrary.com](https://onlinelibrary.wiley.com/doi/10.1002/app.54320)]

a movement of the charge carriers within the polymer, that is, motion of ions and an alignment of dipoles. An alternating current with a phase shift relative to the applied voltage results, which characterizes the ion and dipole mobility. It allows to calculate the ion viscosity and the relative permittivity of the polymer. Figure 9 shows the real-time in-mold ionic viscosity as function of time close to the sprue and at fringe of the mold during a T-RTM process (geometry of the mold see Reference 63). The dielectric sensors allow for the characterization of the flow-front arrival (first drop of dielectric signal), the injection process and the flow behavior (minimal ion viscosity), and the solidification due to polymerization and crystallization (increase of ion viscosity). The temporal shift between the two signals demonstrates the course of the flow-front, which first passes at the sprue and then arrives at the fringe. In addition to the DEA signal, the temperature is monitored. The only small temperature changes of about 3°C at the sprue and 2°C at the fringe demonstrate the thermal stability of the system.

The polymerization and the partially overlapping crystallization process is characterized by a decrease of mobility and an increase of polarizability. The relative permittivity is a quantity that can follow both (see Figure 10).

The time interval starting with the maximum value of permittivity at roughly 4 min up to the minimum around 4.5 min is dominated by the polymerization, whereas the subsequent increase of permittivity is dominated by the crystallization.

Finally, the measured dielectric signal can be used to calculate the degree of total conversion in real-time. To this end, the kinetic model predicts the concentration of monomers as a function of time and temperature. The

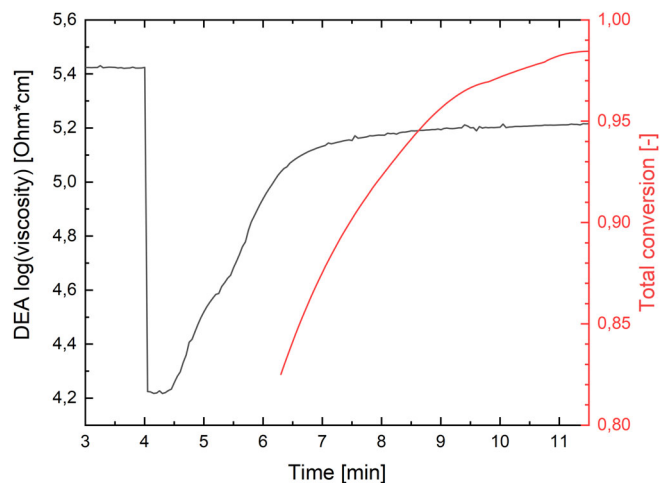


FIGURE 11 Ion viscosity at 100 kHz and total conversion calculated by the kinetic model. [Color figure can be viewed at [wileyonlinelibrary.com](https://onlinelibrary.wiley.com/doi/10.1002/app.54320)]

monomer concentration determines the ion viscosity of the system. Combining the two, the conversion as function of time can be determined. Both, the measured DEA signal and the resulting prediction of the conversion are shown in Figure 11. This allows to control cycle times and to increase the efficiency during component manufacturing using the T-RTM process. Such an inline monitoring of the manufacturing process can help to recognize process deviations and therefore to automatically adapt production in real-time. This concept, developed in the funded project CosiMo, has now become commercially available within the solution of sensXPRT provided by Netzsch Process Intelligence.

4 | CONCLUSION

Applying a specially adapted DSC temperature program, it was possible to investigate the anionic polymerization of ϵ -CL to PA6 quasi-isothermally. The influence of the reaction temperature on the released enthalpies was shown. It was found that the polymerization rate increases with increasing temperature and that anionic polymerization proceeds faster. At the same time, the degree of crystallization of the synthesized PA6 decreases with increasing temperature. A maximum of the polymerization enthalpy, and thus probably the highest conversion, is observed at 150°C.

Using an optimized isothermal DSC measurement, a semi-empirical two-stage kinetic model for the solvent-based material system of the manufacturer Katchem was established for the first time. With a coupled modeling of polymerization and crystallization a very good fit of the kinetic model to the total conversion of the isothermal

DSC measurement data was achieved. The resulting parameters of the Kamal-Sourour equation for polymerization agree with values from the literature.

This kinetic model was finally coupled with dielectric sensor data for application in the T-RTM process. This enables real-time prediction of total conversion.

AUTHOR CONTRIBUTIONS

Samet Kurt: Project administration (lead); writing – original draft (lead); writing – review and editing (lead). **Thomas Bratzdrum:** Investigation (supporting). **Alexander Chaloupka:** Software (lead); writing – review and editing (supporting). **Siegfried Horn:** Writing – review and editing (equal). **Judith Moosburger-Will:** Project administration (equal); writing – review and editing (equal).

ACKNOWLEDGMENTS

We acknowledge the support of the Bavarian Ministry of Economic Affairs, Regional Development and Energy through the program “New Materials in Bavaria” (funding number NW-1803-0013) and Brüggemann Chemical, Germany and Katchem spol. s r.o, Czech Republic for kindly supplying the additives and the monomer. Open Access funding enabled and organized by Projekt DEAL.

DATA AVAILABILITY STATEMENT

The data that support the findings of this study are available on request from the corresponding author. The data are not publicly available due to privacy or ethical restrictions.

ORCID

Samet Kurt  <https://orcid.org/0000-0003-1662-956X>

Alexander Chaloupka  <https://orcid.org/0000-0002-3305-1045>

Siegfried Horn  <https://orcid.org/0000-0002-8379-7283>

Judith Moosburger-Will  <https://orcid.org/0000-0001-9137-980X>

REFERENCES

- [1] I. Sibikin, J. Karger-Kocsis, *Adv. Indus. Eng. Polym. Res.* **2018**, *1*, 48.
- [2] K. van Rijswijk, H. Bersee, *Compos. A Appl. Sci. Manuf.* **2007**, *38*, 666.
- [3] T. Ageyeva, I. Sibikin, J. Karger-Kocsis, *Polymer* **2018**, *10*, 357.
- [4] S. Pillay, U. K. Vaidya, G. M. Janowski, *J. Thermoplast. Compos. Mater.* **2005**, *18*, 509.
- [5] R. S. Davé, R. L. Kruse, K. Udiipi, D. E. Williams, *Polymer* **1997**, *38*, 949.
- [6] N. Dencheva, Z. Denchev, A. S. Pouzada, A. S. Sampaio, A. M. Rocha, *J. Mater. Sci.* **2013**, *48*, 7260.
- [7] K. van Rijswijk, H. Bersee, A. Beukers, S. J. Picken, A. A. van Geenen, *Polym. Test.* **2006**, *25*, 392.
- [8] K. van Rijswijk, H. Bersee, W. F. Jager, S. J. Picken, *Compos. A Appl. Sci. Manuf.* **2006**, *37*, 949.
- [9] J. Humphry, N. Yang, L.-J. Vandi, B. V. Hernandez, D. J. Martin, M. T. Heitzmann, *Mater. Today Commun.* **2020**, *25*, 101473.
- [10] S. Russo, S. Maniscalco, P. Moretti, L. Ricco, *J. Polym. Sci. A Polym. Chem.* **2013**, *51*, 4474.
- [11] K. Khodabakhshi, M. Gilbert, P. Dickens, *Polym. Adv. Technol.* **2013**, *24*, 503.
- [12] C. Vicard, O. de Almeida, A. Cantarel, G. Bernhart, *Polymer* **2019**, *180*, 121681.
- [13] R. S. Davé, R. L. Kruse, L. R. Stebbins, K. Udiipi, *Polymer* **1997**, *38*, 939.
- [14] N. Barhoumi, A. Maazouz, M. Jaziri, R. Abdelhedi, *Exp. Polym. Lett.* **2013**, *7*, 76.
- [15] A. Maazouz, K. Lamnawar, M. Dkier, *Compos. A Appl. Sci. Manuf.* **2018**, *107*, 235.
- [16] L. Ricco, S. Russo, G. Orefice, F. Riva, *Macromolecules* **1999**, *32*, 7726.
- [17] K. Udiipi, R. S. Davé, R. L. Kruse, L. R. Stebbins, *Polymer* **1997**, *38*, 927.
- [18] M.-X. Li, D. Lee, G. H. Lee, S. M. Kim, G. Ben, W. I. Lee, S. W. Choi, *Polymer* **2020**, *12*, 947.
- [19] M. Wilhelm, R. Wendel, M. Aust, P. Rosenberg, F. Henning, *J. Compos. Sci.* **2020**, *4*, 7.
- [20] R. Wendel, P. Rosenberg, M. Wilhelm, F. Henning, *J. Compos. Sci.* **2020**, *4*, 8.
- [21] R. Wendel, B. Thoma, F. Henning. Polymer Processing Society (PPS International Conference) 2017.
- [22] P. Bernat, O. Hladká, M. Fišmanová, J. Roda, J. Brožek, *Eur. Polym. J.* **2008**, *44*, 32.
- [23] C. Vicard, O. de Almeida, A. Cantarel, G. Bernhart, *Polymer* **2017**, *132*, 88.
- [24] K. Taki, N. Shoji, M. Kobayashi, H. Ito, *Microsyst. Technol.* **2017**, *23*, 1161.
- [25] J. J. E. Teuwen, A. A. van Geenen, H. E. N. Bersee, *Macromol. Mater. Eng.* **2013**, *298*, 163.
- [26] T. Ageyeva, I. Sibikin, J. G. Kovács, *Polymer* **2019**, *11*, 1555.
- [27] A. Rigo, G. Fabbri, G. Talamini, *J. Polym. Sci. B Polym. Lett. Ed.* **1975**, *13*, 469.
- [28] E. Šittler, J. Šebenda, *Collect. Czech. Chem. Commun.* **1968**, *33*, 270.
- [29] R. Z. Greenley, J. C. Stauffer, J. E. Kurz, *Macromolecules* **1969**, *2*, 561.
- [30] D. J. Lin, J. M. Ottino, E. L. Thomas, *Polym. Eng. Sci.* **1985**, *25*, 1155.
- [31] R. A. Cimini, D. C. Sundberg, *Polym. Eng. Sci.* **1986**, *26*, 560.
- [32] S. A. Bolgov, V. P. Begishev, A. Malkin, V. G. Frolov, *Polym. Sci. U.S.S.R.* **1981**, *23*, 1485.
- [33] A. Malkin, V. P. Beghishev, S. A. Bolgov, *Polimeros* **1982**, *23*, 385.
- [34] P. Wittmer, H. Gerrens, *Makromol. Chem.* **1965**, *89*, 27.
- [35] A. Malkin, V. G. Frolov, A. N. Ivanova, Z. S. Andrianova, *Polym. Sci. U.S.S.R.* **1979**, *21*, 691.
- [36] A. Malkin, S. L. Ivanova, V. G. Frolov, A. N. Ivanova, Z. S. Andrianova, *Polimeros* **1982**, *23*, 1791.
- [37] M. R. Kamal, S. Sourour, *Polym. Eng. Sci.* **1973**, *13*, 59.
- [38] S. Sourour, M. R. Kamal, *Thermochim. Acta* **1976**, *14*, 41.
- [39] T. A. Osswald, G. Menges, *Materials Science of Polymers for Engineers*, Carl Hanser Verlag GmbH & Co. KG, München **2012**.

- [40] A. Malkin, V. G. Frolov, A. N. Ivanova, Z. S. Andrianova, L. A. Alekseichenko, *Polym. Sci. U.S.S.R.* **1980**, *22*, 1097.
- [41] A. Malkin, S. G. Kulichikhin, A. E. Chalykh, *Polimeros* **1981**, *22*, 1373.
- [42] R. E. Camargo, V. M. Gonzalez, C. W. Macosko, M. Tirrell, *Rubber Chem. Technol.* **1983**, *56*, 774.
- [43] J. D. Hoffman, J. I. Lauritzen, *Section A, Phys. Chem.* **1961**, *65A*, 297.
- [44] M. Avrami, *J. Chem. Phys.* **1940**, *8*, 212.
- [45] M. Avrami, *J. Chem. Phys.* **1941**, *9*, 177.
- [46] M. Avrami, *J. Chem. Phys.* **1939**, *7*, 1103.
- [47] A. Y. Malkin, V. P. Beghishev, I. A. Keapin, Z. S. Andrianova, *Polym. Eng. Sci.* **1984**, *24*, 1402.
- [48] A. Y. Malkin, V. P. Beghishev, I. A. Keapin, S. A. Bolgov, *Polym. Eng. Sci.* **1984**, *24*, 1396.
- [49] A. Malkin, V. P. Beghishev, I. A. Keapin, *Polimeros* **1983**, *24*, 81.
- [50] K. H. Lee, S. C. Kim, *Polym. Eng. Sci.* **1988**, *28*, 13.
- [51] K. Nakamura, K. Katayama, T. Amano, *J. Appl. Polym. Sci.* **1973**, *17*, 1031.
- [52] K. Nakamura, T. Watanabe, K. Katayama, T. Amano, *J. Appl. Polym. Sci.* **1972**, *16*, 1077.
- [53] R. M. Patel, J. E. Spruiell, *Polym. Eng. Sci.* **1991**, *31*, 730.
- [54] C. Vicard. 21st International Conference on Composite Materials. **2017**.
- [55] J. Karger-Kocsis, L. Kiss, *Makromol. Chem.* **1979**, *180*, 1593.
- [56] K.-H. Illers, *Makromol. Chem.* **1978**, *179*, 497.
- [57] T. D. Fornes, D. R. Paul, *Polymer* **2003**, *44*, 3945.
- [58] D. L. Wilfong, C. A. Pommerening, Z. G. Gardlund, *Polimeros* **1992**, *33*, 3884.
- [59] T. Komoto, M. Iguchi, H. Kanetsuna, T. Kawai, *Makromol. Chem.* **1970**, *135*, 145.
- [60] K. van Rijswijk, A. A. van Geenen, H. Bersee, *Compos. A Appl. Sci. Manuf.* **2009**, *40*, 1033.
- [61] K. J. Kim, Y. Y. Kim, B. S. Yoon, K. J. Yoon, *J. Appl. Polym. Sci.* **1995**, *57*, 1347.
- [62] J. Humphry, N. Wolter, N. Yang, L.-J. Vandi, R. Truss, D. J. Martin, M. T. Heitzmann, *Compos. Commun.* **2018**, *8*, 111.
- [63] J. Faber, M. Vistein, A. Chaloupka, M. Achzet, F. Linscheid, S. Kurt, M. Sause. SAMPE Europe Conference. **2021**.

How to cite this article: S. Kurt, T. Bratzdrum, A. Chaloupka, S. Horn, J. Moosburger-Will, *J. Appl. Polym. Sci.* **2023**, e54320. <https://doi.org/10.1002/app.54320>